JOURNAL OF MATERIALS SCIENCE **37** (2002) 1283–1293

Microindentation induced debonding of polymer thin films from rigid substrates

Y. LU, D. M. SHINOZAKI*
Department of Mechanical and Materials Engineering,
The University of Western Ontario, London, Canada N6A 5B9
E-mail: Shinozaki@uwo.ca

A microindenter in the form of a flat cylindrical punch (10 μm < diameter < 100 μm) is used to measure the interfacial shear strength of polymer coatings on relatively rigid substrates. The penetration of the displacement controlled tip in the polymer results in a plastic zone ahead of the moving tip, which generates a large interfacial shear stress. An analysis based on a modified shear lag model can be used to estimate the critical shear stress at which failure of the interface initiates. The test can be used for hard and soft polymers such as polymethylmethacrylate, polystyrene and high impact polystyrene. The thickness of coating which can be tested is shown to be approximately equal to the diameter of the tip.

1. Introduction

Polymer films are widely used as protective coatings on relatively rigid substrates such as ceramics or metals. In many cases, to fulfill its designed purpose, the polymer film must adhere strongly to the substrate. Indentation can be used to generate local debonding, if the mechanics can be described accurately and the conditions for decohesion can be quantified [1]. The failure of the interface involves initiation and propagation of the crack. For hard films, the propagation of the interface crack is driven by the strain energy release rate resulting from the tensile stresses acting normal to the interface which cause the film to buckle [2]. Marshall and Evans propose that the Vickers indentation pushes the material radially outwards from the point of indentation. Compressive stresses cause the buckling in the film as the crack propagates [3]. This approach is also applied to the ZnO/Si interface fracture by Rossington *et al.* [4].

Matthewson analyzes the failure of an interface by proposing that the radial displacement of the material resulting from the indentation with a spherical indenter produces a shear stress at the interface which causes the crack to nucleate and grow [5, 6]. The soft coating is assumed to yield according to a Tresca criterion, and does not work harden. The radial stress is then equal to the yield stress (σ_y) of the material. The measured indentation stress is then assumed to be $> 3\sigma_y$ for a thin film constrained by the rigid substrate. The analysis is most accurate for $a/h > 2$, where a is the contact radius of the spherical indenter and h is the coating thickness. The same approach is used by Ritter *et al.* and compared to an elastic finite element model [7].

Vratsanos *et al.* show that the interface shear strength is sensitive to the normal component of the stress field, and the failure follows a modified Tsai-Wu criterion [8]. Interface fracture is unlikely to initiate directly under the contact area, where the normal stress is large and compressive (suppressing crack opening).

The use of flat punch geometry in microindentation testing is less common, with some earlier work reported by Li and co-workers [9–12], and the more recent work of Cheng and co-workers [1]. These papers looked mainly at the creep and viscoelastic deformation of soft materials. Plastic flow around a flat faced cylindrical punch has been examined by Wright *et al.* for deep penetration of macroindenters in polycarbonate [13]. This analysis was based on the very early studies of Bishop *et al.* [14]. A similar approach has been used to analyze microindentation at constant penetration rates for polyethylene [15]. The analysis showed that specific material properties (work hardening characteristics which are dependent on deformation rate and microstructure) could be inferred from the flat punch penetration test. Viscoelastic properties in polymers have also been measured using this tip geometry by restricting the penetration to the near surface region, and oscillating the tip through extremely small amplitude sinusoidal displacements [16, 17].

The use of flat punch geometry has an advantage over tapered or spherical geometries because the contact loading area remains constant even for deep penetration. The stress and strain fields which develop with increasing penetration eventually reach a steady state shape for specimens large with respect to the tip diameter. With the nearby presence of a relatively rigid substrate adhering strongly to the polymer coating, the stress field under the tip is affected, and the measured forces on the tip are consequently changed. The experimentally measured forces thus can be analyzed in terms of the adhesion strength of the rigid substrate.

---

*Author to whom all correspondence should be addressed.

The present experiments examine the microindentation induced failure of this interface using a small diameter flat punch indenter, with an analysis which follows from the earlier deep penetration tests.

2. Experimental

The polymers used in this work were atactic polystyrene (PS), polymethylmethacrylate (PMMA) and high impact polystyrene (HIPS). These can be prepared in very uniform, smooth thin films on smooth substrates using solution casting. Solvents used were toluene ($C_6H_5CH_3$) for the PS and HIPS and chlorobenzene (C_6H_5Cl) for the PMMA. The concentrations varied in the range 5–25% w/v depending on the thickness needed.

The substrates included silicon, glass, steel, aluminum and copper. Most of the detailed modelling was based on experiments using the first two substrates, which could be prepared in very reproducible, smooth, large flat areas. The metals were included to illustrate the sensitivity of the measurement method to some practically useful materials.

The single crystal silicon wafers and the glass (microscope slides) were fractured to appropriate dimensions (approximately 10 mm × 10 mm) using a diamond knife, washed first in detergent and subsequently rinsed with isopropyl alcohol. The metal samples, of similar dimensions, were mechanically polished using metallographic preparation methods, with a final polish with 0.05 μm alumina, followed by careful washing with detergent and isopropyl alcohol.

The polymers were cast from solution onto the substrates, and dried in a dust free chamber for at least two days. The central portion of such dried films was found to be suitably flat and uniform in thickness. Transverse optical sectioning was used to measure film thickness and uniformity ($10 < t < 100$ μm).

Thin interlayers with varying mechanical properties were fabricated by mixing different proportions of PS and HIPS in solution, and spin casting a dilute solution using a Headway resist spinner (5000 rpm for 30 seconds). The interlayer thickness was in the range 3–5 μm. After drying, a much thicker layer (approximately 50 μm) of homopolymer PS was cast onto the interlayer. By varying the proportion of PS:HIPS in the interlayer, the rubber phase content could be adjusted from 0 to 10%. The two materials were inherently compatible, so the PS:HIPS interface was relatively well bonded.

The microindenter itself consisted of a cylindrical steel punch, with a diameter in the range $10 < d < 100$ μm prepared by electropolishing cold drawn steel wire. The contact surface of the microindenter was prepared by metallographic polishing using progressively smaller polishing compounds to 0.05 μm Al_2O_3. The size and shape of the tip was confirmed with appropriate microscopy. The tip was attached to the piezoelectric driver, the position of which was controlled through a strain gauge monitor attached to the piezoelectric driver. The load cell signal was measured through a bridge amplifier. The displacement was controlled to be linear with time, with variable rate between 1 to 24 μm/min. For the present experiments, an indenter velocity of 2.4 μm/min was used. The data acquisition and instrument control were handled using LABVIEW using GPIB interfacing with the electronics.

The tensile properties of thin samples were measured using a specially constructed microtensile tester. This consisted of a horizontally driven optical stage, with suitable load cell and computer control. The horizontal configuration was found to be much more convenient for the mounting of the extremely thin samples.

3. Results and discussion

3.1. Phenomenology of microindentation of unconstrained polymers

The microindentation stress-displacement curves for the bulk PS, PMMA and HIPS (without substrates) are seen in Fig. 1. The curves for PMMA and PS are similar to each other, with the first being slightly harder, while the HIPS is much softer.

The general shapes of the load displacement curves for polymers tested here without a substrate are similar to that seen earlier for high density polyethylene [15]. The microindentation proceeded by contacting the surface of the polymer sample until the initial load could be observed. As the tip face contacts the material, an elastic stress field develops. The stress field can be calculated following Mouginot and Maugis [18] which was based on Sneddon's modelling [19] of a semi-infinite sample indented by a rigid flat ended cylindrical punch. The axial stress (σ_3) is shown in Fig. 2 to drop off with depth below the tip face. Significant axial stresses are seen in the material down to approximately 1 diameter below the tip face. A compressive stress in the radial direction (σ_1) develops (Fig. 3) which pushes the material outwards from beneath the indenter tip. The surrounding material constrains this material movement, resulting in the requirement of a higher axial stress to initiate plastic flow (the familiar constraint factor discussed extensively by Tabor [20–22]).

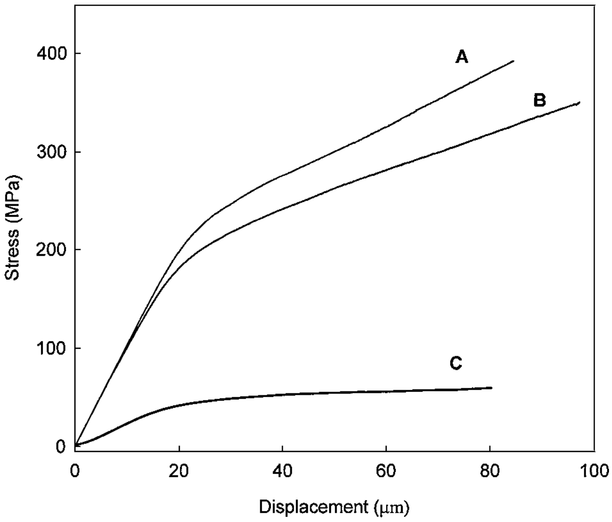

Figure 1 Microindentation tests on (A) PMMA; (B) PS; and (C) HIPS with no adherant substrate. The indenter diameter is 76.2 μm. The stress is the (applied force)/(tip area).

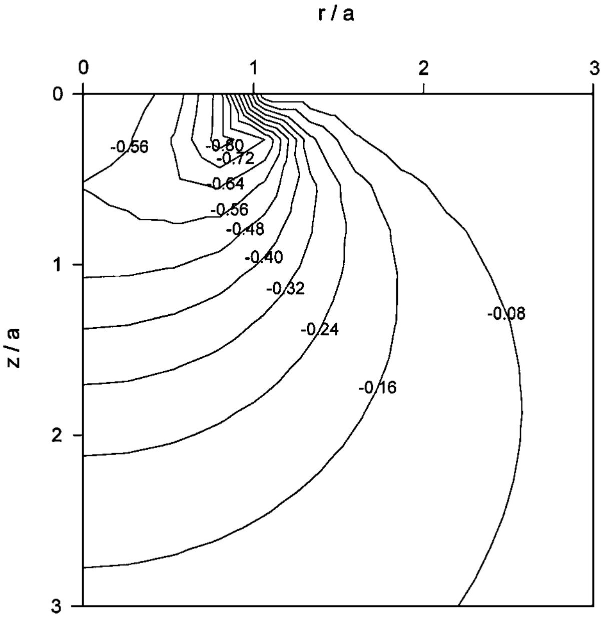

Figure 2 Stress in the axial direction (σ_3) under a cylindrical indenter after Sneddon [1946]. The radial direction is r and the axial direction is z. Both are normalized with respect to the radius of the indenter a. The stresses are normalized with respect to the applied stress.

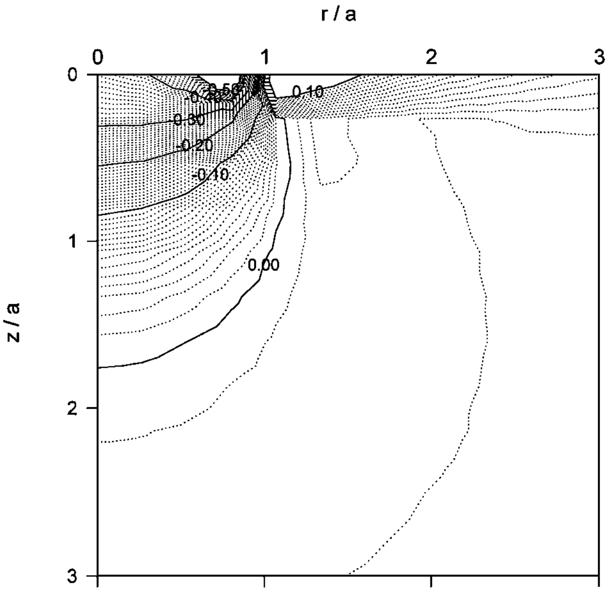

Figure 3 Stress in the radial direction (σ_1) under a cylindrical indenter after Sneddon [1946].

As the indenter is pressed further into the surface, the stress increases proportionately to the nominal punch stress, until the material yields, initially near the indenter corner (A) where the octahedral stress is a maximum (Fig. 4). The measured load-displacement curves are shown for unconstrained thick films, in which the thickness is much greater than the tip diameter, and no rigid substrate is present. The punch face progressively penetrates the polymer, displacing material radially.

The development of a full plastic zone is observed to correspond to the knee of the penetration stress-displacement curve (Fig. 1). Beyond the depth at which the knee of the curve is observed, the curve is linear for the relatively hard polymers tested here, similar to results from high density polyethylene [15]. The observation that a steady state zone develops suggests that the penetration force should be constant beyond the knee of the curve: the polymer being pushed away from the region in front of the moving punch face in a continuous process. The experimental curve however shows a linear region of positive slope. The apparent hardening results from the increase in frictional force on the lateral surfaces of the moving cylindrical punch. This has been shown by examining the residual hole left after a deep penetration test, in which the diameter measured immediately after withdrawal was significantly smaller than the indenter diameter. The elastic contraction showed that there was a significant force normal to the indenter lateral surface, and the frictional force retarding the penetration increased linearly with depth (since the surface area in contact with the specimen increased linearly).

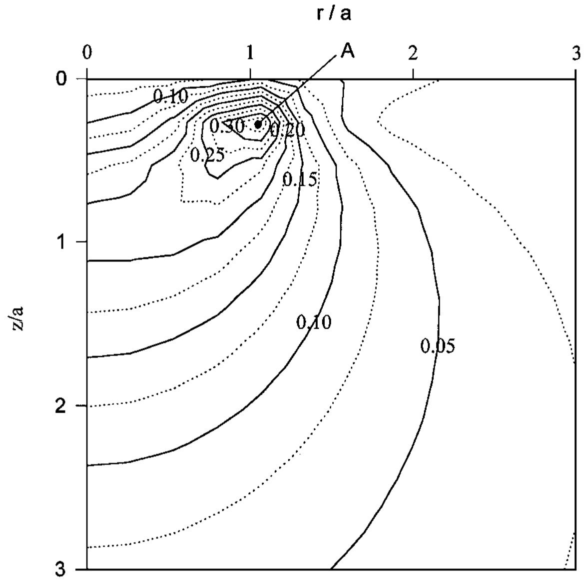

Figure 4 Octahedral stress under a cylindrical indenter after Sneddon [1946].

By extrapolating the linear part of the large displacement curve back to the vertical axis and measuring the intercept with this axis, the critical indentation stress (P_m) of the material can be calculated. P_m is a measure of the yield strength, modified by a "constraint factor" which arises from the containment of the plastically deforming volume by the surrounding elastically deformed material [15]. The indentation stresses so measured are consistent with the yield strength of the coating materials obtained from the micro-tensile tester (Table I).

For the spherulitic high density polyethylene sample tested in earlier work, with increasing penetration the yielded zone spreads below the indenter over a curved

TABLE I Comparison of indentation stress (P_m) and tensile yield strength (σ_y)

	P_m (MPa)	σ_y (MPa)	P_m/σ_y
PS	166.2	60	2.70
PMMA	175.8	65	2.77
HIPS	41.5	15	2.76

conical surface with a half angle of less than 45°, presumably following the region of maximum shear stress. The further penetration of the indenter ($z > d$, where z is the depth of penetration and d is the diameter of the cylindrical indenter) results in a mechanical steady state, where the polyethylene is pushed away from the region directly under the indenter. In this unconstrained case the large plastic strains develop in the zone a distance of approximately 1 diameter below the indenter face. For the present experiments in which the strength of the interface with an adherent substrate is to be measured, the specimen geometry was designed so that the interface of interest lay within a distance of 1 diameter from the tip face.

High density polyethylene tested in the earlier work shows a strong dependence on crystallinity, with quenched material being much softer and highly crystalline samples being considerably harder than PMMA and PS. The known dependence of the microindentation test data on material properties and test parameters dictated that the debonding measurements in the present experiments be made at a specific displacement rate for a given tip diameter. The reason for this is explained as follows.

The effective strain rate imposed on the polymer is directly related to the displacement rate of the microindenter. The force on the microindenter is related to the effective plastic resistance of the polymer at the experimentally fixed displacement rate of the tip. Assuming a positive relationship between the plastic resistance and the local material strain rate, the region of the specimen which limits the tip velocity is that which is subjected to the maximum strain rate. This limiting effective material strain rate ($\dot{\varepsilon}_{\text{eff}}$) was suggested by Li to be $v/2a$ [10], and by Sargent and Ashby as $v/\sqrt{A}$ [23], where v is the tip velocity and A is the crossectional area of the indenter. Earlier work has shown that the Sargent and Ashby approximation was closest to the experimental results [15].

For the debonding experiments, it is therefore important to use a constant tip velocity. Typical hardness testing which imposes a fixed loading rate or a fixed load produces widely varying strain rates in the polymer. The interfacial shear stress depends on the applied punch stress and the material properties (yield stress, work hardening rate) which are in turn strongly dependent on the strain rate. The measured microindenter force at debonding thus depends on the applied displacement rate.

3.2. Microindentation of polymer films attached to substrates

In the case of polymer coatings adhering to a stiff substrate, the material being pushed aside by the moving indenter is constrained by the adherent substrate. An example of the measured stress-displacement curve for PMMA is shown in Fig. 5a. Comparison with unconstrained PMMA shows that the effect of the constraint is to shift the plastic part of the indentation curve to higher stresses and to reduce the plastic relaxation rate [15]. The stress-displacement curves are closely reproducible for a given specimen. A series of separate penetration tests was performed in a sequence to different depths. For example to the points A and B in Fig. 5a (only two points are shown here, although in total 5 tests were used). The letters A and B represent the points on the stress-displacement curve for which the micrographs in Fig. 5b were recorded (after the indenter was withdrawn).

At A, before the stress drop, a small annular region with a diameter of approximately twice that of the residual hole was observed. The sudden load drop seen in Fig. 5a at a depth of approximately 25 μm is due to the initiation of a circular decohesion zone at the interface

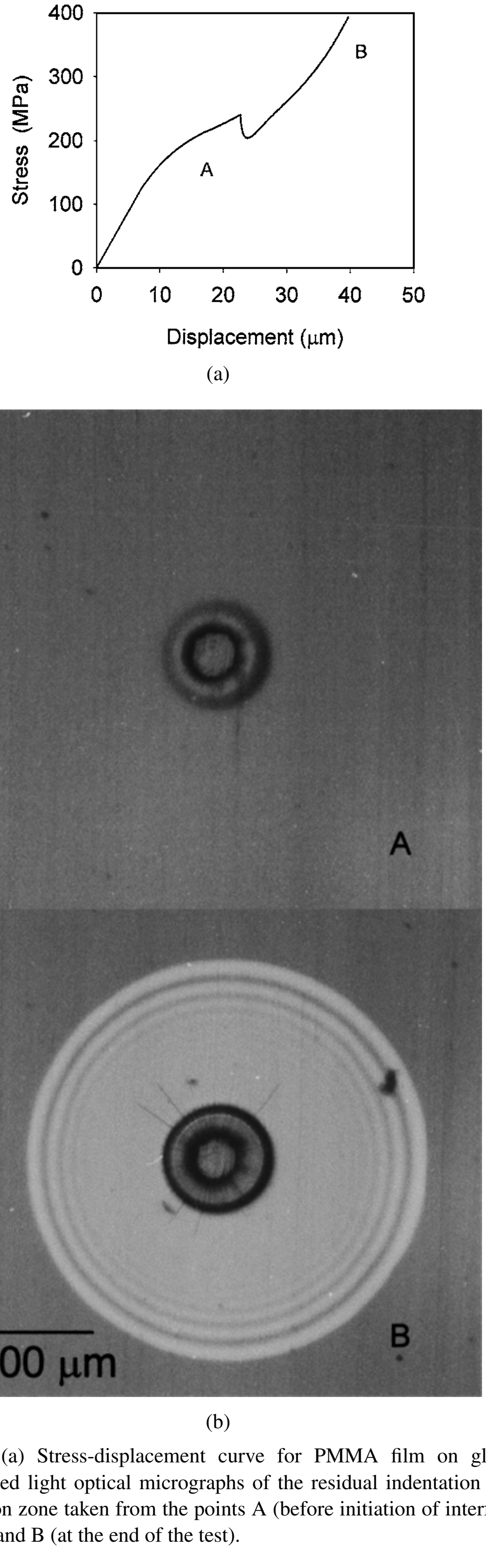

(a)

(b)

Figure 5 (a) Stress-displacement curve for PMMA film on glass; (b) reflected light optical micrographs of the residual indentation and decohesion zone taken from the points A (before initiation of interface fracture) and B (at the end of the test).

TABLE II The critical indentation debonding stress and depth as determined from indentation stress-displacement curves

	Coating thickness h_f (μm)	Critical indentation debonding stress P_c (N)	Critical indentation debonding depth h_c (μm)
PS-Silicon	50.6 (1.02)	193.77 (2.12)	17.586 (1.14)
PS-Glass	49.8 (0.26)	201.11 (2.23)	15.677 (1.18)
PS-Steel	50.5 (0.23)	162.22 (4.04)	18.534 (1.65)
PS-Copper	51.2 (1.35)	163.33 (3.36)	15.664 (1.63)
PS-Aluminum	48.8 (1.30)	179.78 (3.15)	14.899 (0.72)
PMMA-Silicon	52.5 (1.01)	223.11 (2.87)	27.34 (1.35)
PMMA-Glass	50.7 (0.56)	223.56 (2.32)	26.38 (1.62)

Each number represents an average of 6 indentations.
Number in parenthesis represents ± one standard deviation.

which can be observed directly using an in situ optical microscope. With further penetration, the radius of the decohesion zone increases, reaching some limiting value as the indenter approaches the substrate and the polymer becomes fully constrained by the interface friction, seen in Fig. 5b (B).

The load drop shown in Fig. 5a is a result of the relaxation of the axial stress as the crack propagates at the interface (for a relatively stiff microindenter). The crack stops when the local crack tip stress falls below some critical value. After the crack is initiated, further penetration of the indenter causes further crack growth with no obvious discrete change in the stress-displacement curve. The stress increases at an increasing rate, due to the constraint of the polymer between the indenter and substrate.

From indentation stress-displacement curves of the form described above, the critical indentation debonding stress, P_c, and critical indentation debonding depth, h_c, were measured for PMMA and PS coatings (Table II). The good reproducibility of the test results is shown by the standard deviation of the measured data. The values in Table II are used later to estimate the critical interface failure strength.

Unloading to zero load after the initial interface fracture event, and immediately reloading results in another load drop, albeit smaller and more diffuse (relatively slow load drop) than the initial one. This is seen in the example of PS on glass (Fig. 6). The radius of the delaminated zone reaches a saturation limit at an applied nominal stress of approximately 280 MPa, beyond which the constraint effect restricts further radial extrusion.

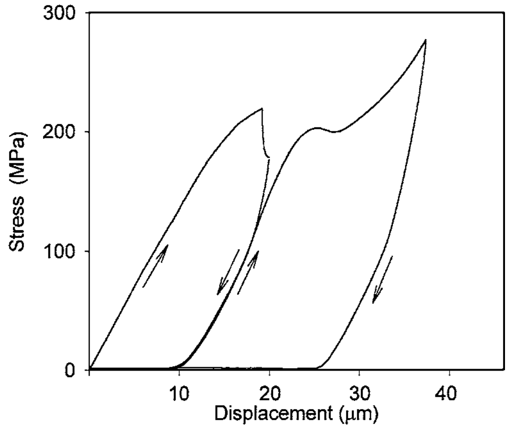

Figure 6 Loading-unloading test on PS adhering to glass. The first unloading starts immediately after load drop.

The decohesion phenomenology for PS coatings is similar to that for PMMA. The micrographs of Fig. 7a were taken from the points A, B and C of the stress-displacement curve (Fig. 7b) and show the increase in diameter of the decohesion zone with increasing penetration of the indenter. The major difference from the PS films of Fig. 5b is the observation of radial cracks (Fig. 7a). Optical microscopic observation of the region near the indentation during testing showed that the radial cracks appeared before the critical interface debonding, but no corresponding load drop was associated with the initiation of radial cracking.

The reason for this radial cracking in PS can be inferred from finite element modelling. Using the ABAQUS, the stress field surrounding the indenter has been calculated [24]. The hoop stress reaches a maximum (tensile) stress at the free surface approximately 1 radius away from the projected position of the outer rim of the indenter. The material under the indenter extrudes radically outwards and a compressive stress field develops in the region near the interface. The radial cracks which develop in PS during penetration clearly initiate in the surface layers away from the interface itself.

It is expected that the radial cracking relaxes the compressive stress field at the interface to some extent. However it is shown later in this paper that the analysis using a modified Dehm model assumes no constraint in the surface region, and the predicted results are not affected by the change in surface constraint.

The transmitted light micrograph of a microindentation under crossed polars shows a sharply defined annulus ($a < r < 2r$) immediately surrounding the indentation hole (Fig. 8). It has a distinct contrast compared to the background, with extinction lines characteristic of birefringent contrast due to either the molecular orientation or to the residual elastic strains. This annular zone consists of material which has been oriented to some extent by plastic deformation, although as discussed above the extremely large plastic strains are more highly localized in the region close to the indenter surface, and the contrast observed here is more likely consistent with stored elastic strains.

3.3. Measurement of interfacial shear strength using microindentation

The point of interface failure can be identified from the microindenter test (Figs 5 and 7). This suggested a method calculating the interface shear strength using a modified version of the Dehm analysis as follows.

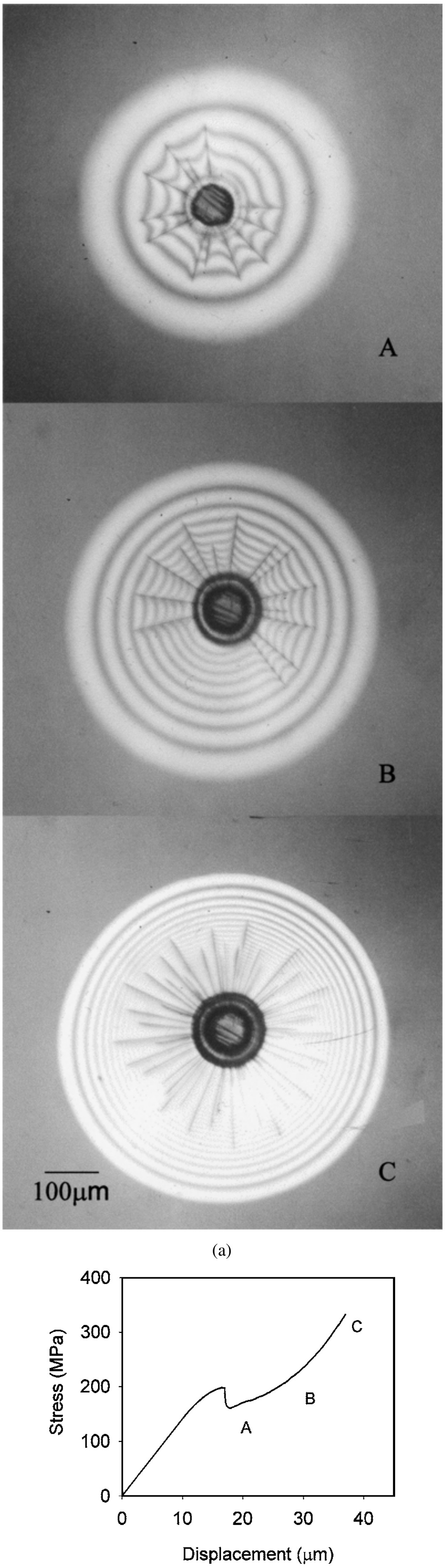

(a)

(b)

Figure 7 (a) Growth of decohesion zone with increasing penetration (PS on glass) (b) stress-displacement curve with points A,B and C corresponding to micrographs.

Dehm *et al.* have presented a simple method for estimating the interfacial strength of copper coatings (500–1100 nm) on rigid sapphire substrates [25]. Using a Vickers indenter, an elastic model of the stresses was developed in which the pressure applied by the indenter (P) was related to the radial stress (σ_r). A simplifying assumption was that the axial and radial stresses were uniformly distributed under the projected contact area. The interfacial shear stress (τ) just outside the projected contact area was furthermore assumed to follow a shear lag model with the stress increasing sinusoidally with radial distance. Imposing mechanical equilibrium then results in a relationship between the applied indenter force, the interfacial shear stress and the depth of penetration. For the materials tested, an increase in interfacial shear strength was manifested as an overall increase in force-displacement ("hardness") curve.

A modified version of the Dehm' model was applied here to the cylindrical, flat shaped indenter. In Fig. 9, the deformation under the flat axisymmetric indenter is divided into three zones (in the radial direction): the region directly under the punch face (AAAA); an annular region (BCAA) immediately surrounding the contact zone; and the rest of the material at a larger radial distance. The material under the indenter (AAAA) initially deforms elastically, with a stress field similar to that shown in Figs 2 and 3, with the additional constraint of a relatively stiff adherent substrate at approximately $1.3a$ (where a is the indenter radius). With further penetration, the zone under the indenter yields, and plastically flows outward in the radial direction. If the material does not work harden, these regions deform at the yield stress. Under steady state conditions in which the material flows radically, the stress field consists of a uniform axial stress (P) and inplane biaxial stress, one component of which is the radial stress (σ_r). These are principal stresses related through a yield criterion (Tresca):

$$P - \sigma_r = \sigma_y \tag{1}$$

where σ_y is the yield strength.

The extrusion of polymer in the radial direction is constrained by adhesion to the relatively stiff substrate. The interfacial shear stress is zero at the axial center of the indenter ($r = 0$) and increases to a maximum at some radial distance outside the edge of the indenter ($r > a$), decreasing beyond this point. Following Agarwal and Raj [26], the shear stress in the present case is assumed approximate a sinusoidal function:

$$\tau = \tau_{\max} \sin \frac{\pi r}{(2a + \zeta)}, \qquad (0 \le r \le (2a + \zeta)) \tag{2}$$

where the interfacial shear stress rises and falls over a half wavelength $\lambda_0/2 = 2a + \zeta$, and ζ is the uncertainty in expressing the exact half wavelength distance.

Invoking equilibrium, the radial stress is balanced by the shear stress integrated over the radial distance over which it is significant ($r = 2a + \zeta$). Taking an elemental unit width, this results in:

$$\sigma_r = \frac{1}{h} \int_0^{2a+\zeta} \tau \, \mathrm{d}r = \frac{4(a + \xi)\tau_{\max}}{\pi \cdot h} \tag{3}$$

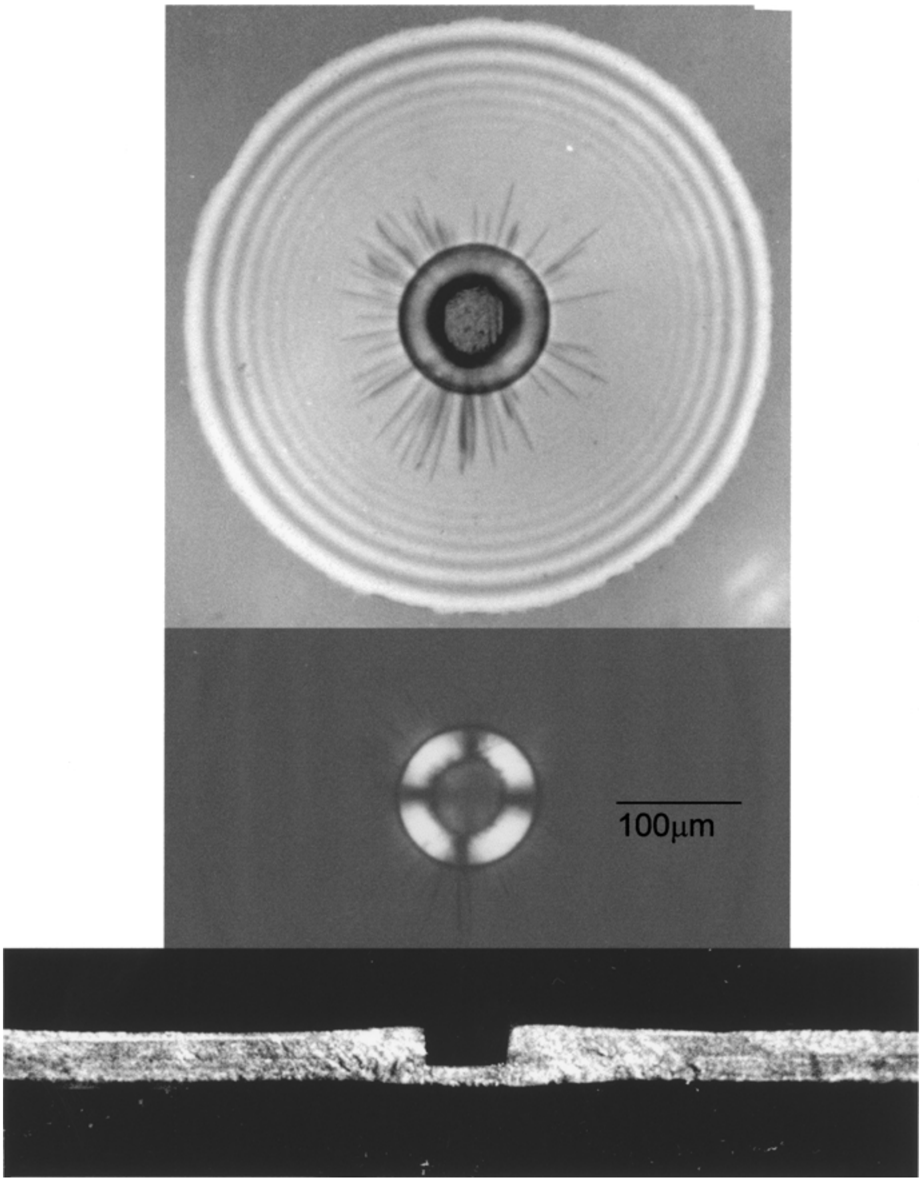

Figure 8 Optical micrographs of microindentation: top to bottom: reflected llight, transmitted light (crossed polars), polished crossection in reflected light.

where ($\xi = \zeta/2$) and h is the thickness of the polymer remaining beneath the indenter tip at the point of failure.

Combining Equations 1 and 3, the maximum interfacial shear stress $\tau_{\max}$ at a given applied indenter stress P is then:

$$\tau_{\max} = \frac{(P - \sigma_y)\pi h}{4(a + \xi)} \qquad (4)$$

In the current study, the maximum shear stress as the interface fails is called the "critical interfacial shear strength", cited as τ_c. Thus Equation 4 is re-written as

$$\tau_c = \frac{(P_c - \sigma_y)\pi h}{4(a + \xi)} \qquad (5)$$

where P_c is the critical indentation stress at debonding; h is the thickness of the residal material beneath the flat-ended punch: $h = h_f - h_c$, where h_f is the coating thickness and h_c is the critical indentation debonding depth. Both P_c and h_c can be measured at the point of interface failure (just before the load drop). The remaining parameter, ξ, can be estimated by examining Fig. 5b, in which the extent of the heavily deformed zone extends out to approximately $2.3a$ to $2.5a$. A much more accurate value can be determined by modelling the indentation using finite elements analysis, yielding a value of $\xi = 0.58a$ for PS, $\xi = 0.59a$ for PMMA and $\xi = 0.55a$ for HIPS, respectively [24]. This suggests that significant interfacial shear stresses beyond the zone of optically obvious heavy deformation.

Using the experimental results (Table II) from the microindentation test, the critical interfacial shear strength (τ_c) for each coating adhering to the glass substrate is calculated using Equation 5, as summarized in Table III.

TABLE III The critical interfacial shear strength (τ_c) calculated using Equation 5

	Interfacial shear strength τ_c (MPa)
PS-Glass	56.9
PMMA-Glass	49.9
HIPS-Glass	11.9

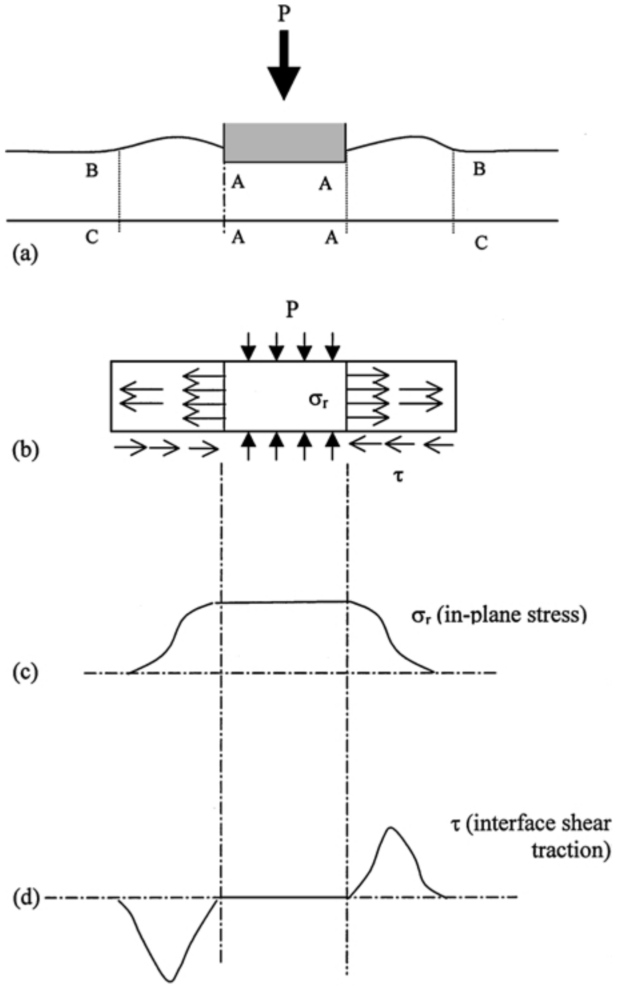

Figure 9 Schematic diagram showing that the shear lag model is applied for the flat face indentation. (a) A cylindrical, flat indenter is indenting a thin coating adhering to substrate. (b) The material in the film immediately underneath the indenter (AAAA) is deformed plastically, and is assumed to consist of a uniform axial pressure P, and an inplane biaxial stress σ_r. (c) The radial stress σ_r in the annular region (BCAA) is assumed to decay gradually. (d) The interfacial shear stress τ is assumed to vary in a sinusoidal shape.

The magnitude of τ_c in Equation 5 mainly depends upon the experimental measurements (P_c and h_c). The earlier results have shown that the variations in P_c and h_c are quite narrow. The averaged standard derivations in P_c and h_c are: $\Delta P_c = \pm 2.7$ MPa, $\Delta h_c = \pm 1.2$ μm. These lead to the errors in P_c and h_c of approximately 1% and 6% respectively. As a result, the error in τ_c is expected to be small.

4. Applications

4.1. Interfacial strength variation for different substrates

The substrates used in the present experiments consist of different kinds of materials: silicon single crystals, glass and metals (aluminum, steel, copper) with Young's moduli and yield stresses much higher than that of the polymers tested. The substrates are all relatively rigid.

The delamination observations and the microindentation stress-displacement curves are found to be similar for all these materials, but the interfacial shear strength (τ_c) varies, as summarized in Table IV (τ_c was calculated using the experimental measurements given in Table II).

TABLE IV The critical interfacial shear strength calculated using Equation 5

	Critical interfacial shear strength τ_c (MPa)
PS-Silicon	57.2
PMMA-Silicon	55.1
HIPS-Silicon	13.9
PS-Steel	42.3
PS-Copper	47.6
PS-Aluminum	52.6

It is observed that the bonding strengths (τ_c) of the polymer coatings to glass and silicon are similar and quite high. In contrast, the bonding strengths of polymer coating (PS) glued on metal substrates are significantly and systematically smaller.

The adhesive strength at the coating-substrate interface, especially at the polymer coating-metal substrate interface varies with a wide variety of chemical and molecular parameters at the interface itself [27]. A study of these is beyond the scope of the present study, which deals only with the development of the test method and its analysis. The primary purpose in using various metal substrates thus is to demonstrate the sensitivity of the indentation technique in distinguishing relatively small differences in interfacial strength. In addition, the relatively small size of the indenter, and of the area of interface tested, can be used to map the distribution of interface shear strength at spatial resolutions a few times larger than the tip diameter.

4.2. Substrate preparation effects

The sensitivity of the test in detecting subtle variations in interface strength is shown in Fig. 10a. Two aluminum surfaces are compared: (a) polished to relatively fine metallographic finish (0.05 μm alumina) and (b) polished to a coarser finish (approximately 3 μm diamond). The smoother surface clearly shows a higher constraint effect and a distinct load drop consistent with harder coatings (Fig. 10a). The associated decohesion zone micrographs (Fig. 10b) show the characteristics of the hard and soft interfaces which distinguish the PS and PMMA from the HIPS coatings. The coarsely polished surface shows a much larger diameter decohesion zone, typical of a weaker interface, with a lower critical fracture load. The interfacial shear strength (τ_c) calculated was 37.4 MPa for this sample, about 15% lower than for the finely polished surface (Table VI), a result consistent with that reported elsewhere [7].

4.3. The effect of soft interlayers

The influence of interlayer on the interfacial adhesion was investigated here, with the initial propose of systematically changing the adhesive strength of the interface in a predictable way. The interlayer consisted of a copolymer which was compatible with the overlayer (PS) and which had variable mechanical properties. The compatibility was provided by the PS component of the copolymer in HIPS. The variations

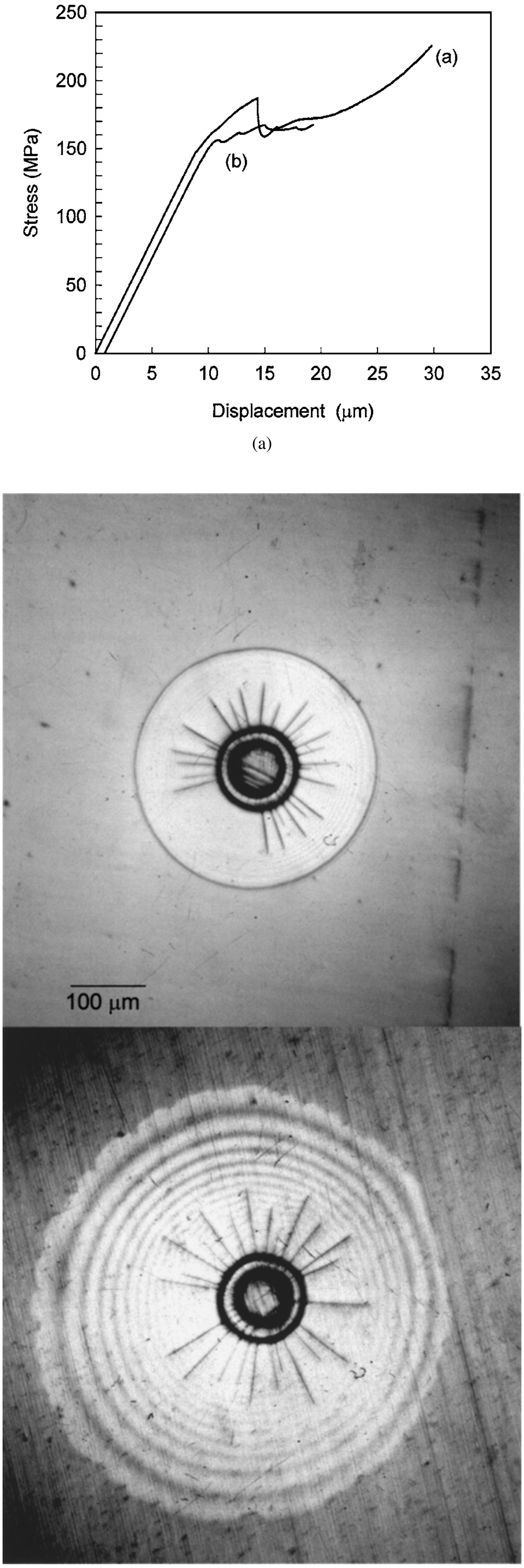

(a)

(b)

Figure 10 (a) Microindentation tests for (a) PS on finely polished Al and (b) PS on coarsely polished Al. (b) Optical micrographs of interface failures. Curve (b) is shifted the right to separate the curves.

in mechanical properties (and adhesive strength) were produced by adjusting the volume fraction of the HIPS in blends of PS and HIPS.

Adhesion between the coating and substrate is the result of interactions between atoms and molecules in a very thin layer (of atomic dimensions) at the interface. Variations in the properties of this layer are expected to result in different values of critical shear strength of the interface. Calculations of the stress field are plotted on a dimensional scale close to the indenter diameter (15–100 μm). At this spatial resolution, the insertion of a thin interlayer film would change the effective strength of the "interface" region, and essentially be close to "zero" thickness. In the present experiments the HIPS interlayer thickness is 1–5 μm. Changes in the interlayer properties appear at the coating thickness scale as apparent changes in the near interface properties.

For soft materials (HIPS), the interface decohesion event is not accompanied by a significant load drop (Fig. 11a). However the interface failure does occur suddenly; detected by direct observation with an optical microscope during the test. The decohesion zone in HIPS is much larger than the harder materials and the fractured interface is rougher on the optical scale (Fig. 11b), indicating residual adhesion of the HIPS on the substrate. This is expected in a two phase material in which the distributed phase is rubbery with a different adhesive strength. It should be pointed out that the visibility of the decohesion point in the load displacement curve depends on the stiffness of the microindenter: increasing the stiffness (especially that of the load cell) would allow for the detection of a load drop. However increasing the load cell stiffness reduces the sensitivity of the load measurement and the signal to noise ratio is reduced.

Five copolymer interlayers were prepared, by varying the rubber content ranging from approximately 0 to 10%. Under the optical microscope, the small rubber particles are clearly visible, distributed evenly in the polystyrene matrix. With the increase of rubber phase content in polystyrene matrix, the mechanical properties of the interlayer change: the yield strength and work hardening characteristics changing as shown in the tensile test curves of Fig. 12.

Fig. 13 displays the indentation stress-displacement response of polystyrene coating on glass substrate with various interlayers. As the rubber content in the interlayer increases, the critical indentation debonding stress P_c progressively decreases. The load drop at the fracture initiation also decreases as the rubber content increases. The results of the critical indentation debonding stress (P_c) and depth (h_c) are summarized in Table V.

Since the thickness of the interlayer is small compared to the film thickness, the coating with an interlayer buried underneath can be treated approximately as one single overlayer with varying interface properties. Thus, Equation 5 derived from the single-layer geometry was used to estimate the "interfacial" shear strength of the multilayer specimens. Using the experimental results (P_c and h_c from the indentation stress-displacement curves), the values of τ_c were calculated, and summarized in Table V. Each measurement was

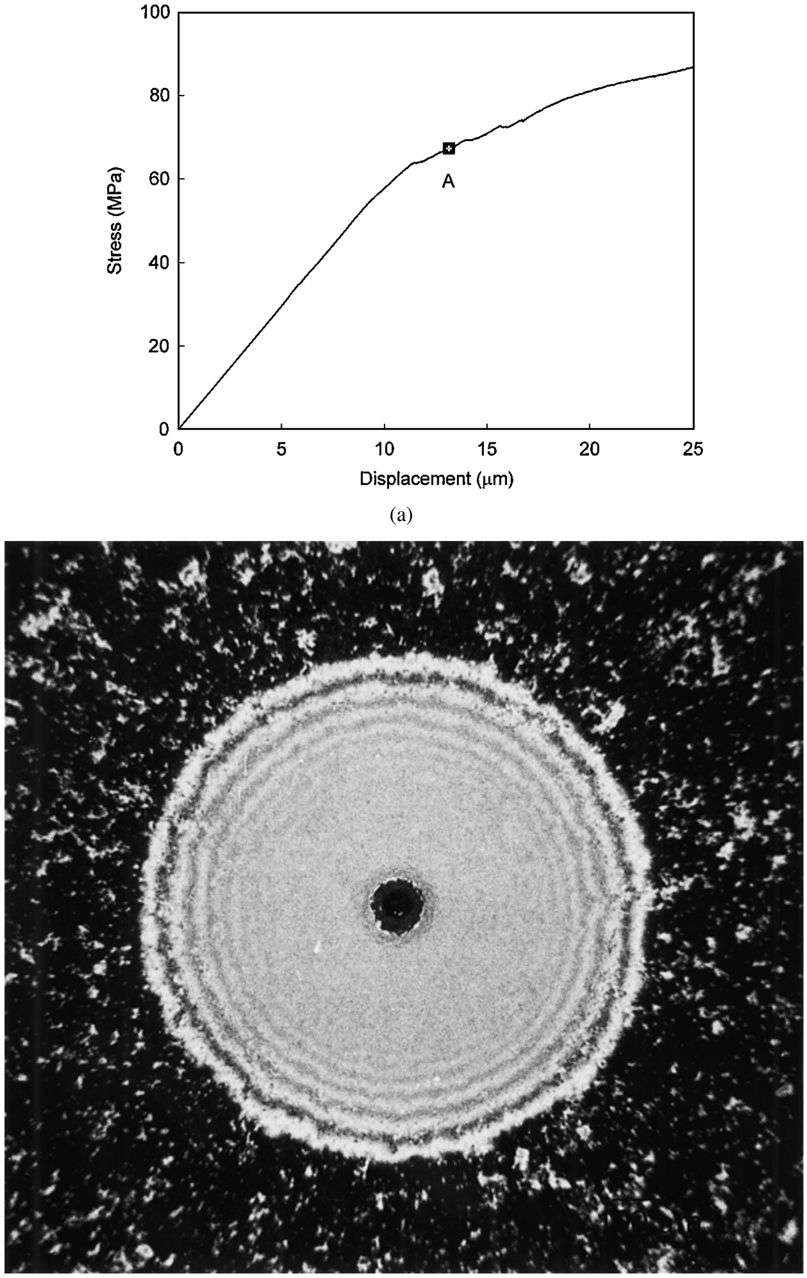

(a)

(b)

Figure 11 (a) Microindentation test of HIPS on glass. The initiation of interface failure is observed optically at the point A. (b) Optical micrograph of decohesion zone in HIPS-glass test. The diameter of the interface fracture zone is larger than for PS or PMMA.

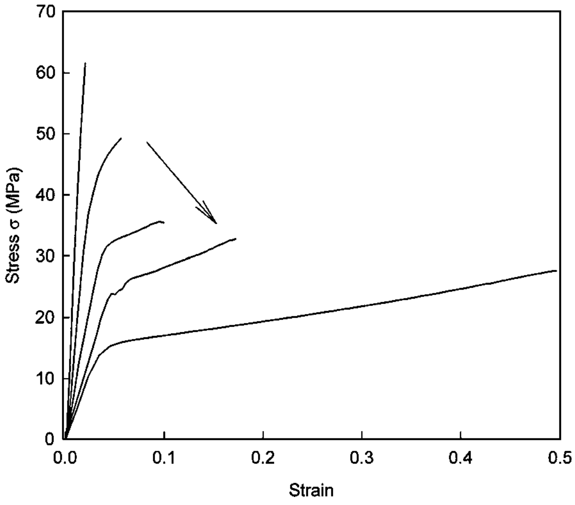

Figure 12 Thin film tensile stress-strain properties of HIPS interlayer materials. The rubber content varies from 0% to 10% (wt), increasing in the direction of the arrow.

TABLE V Effect of interlayer yield strength on the "interfacial" shear strength

Rubber content of the interlayer (% rubber)	[a]Tensile yield strength of interlayer σ_y (MPa)	Interfacial shear strength (PS/Glass) τ_c (MPa)
0.0	60.00	57.3
2.5	48.00	51.8
5.0	35.00	34.0
7.5	30.00	18.2
10	15.00	13.9

[a]The yield strengths of the thin interlayer were determined from a micro-tensile tester.

the average of 6 indentation tests, with excellent reproducibility. For example one standard deviation of the critical debonding stress is less than 2% of the measured value.

It is observed that with an increase of rubber content, τ_c systematically decreased. The magnitude of τ_c

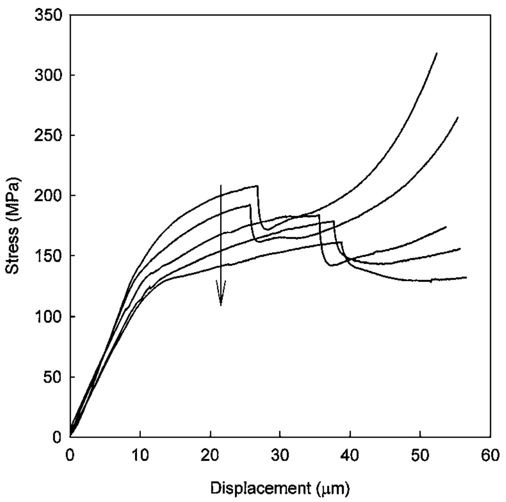

Figure 13 Microindentation curves for PS on glass with a thin soft interlayer (HIPS). The rubbery phase content varies from 0% to 10% (wt), increasing in the direction of the arrow.

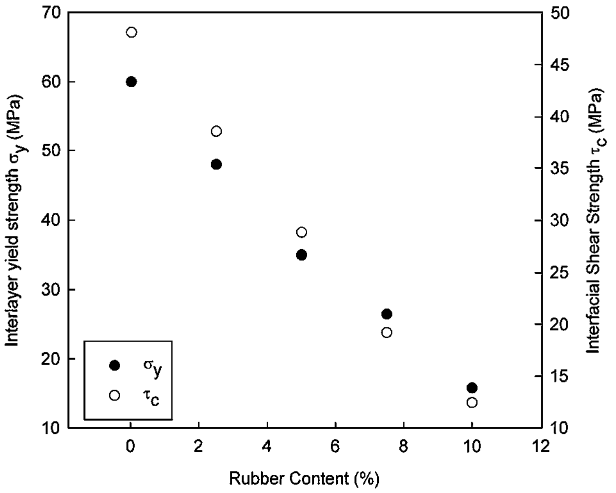

Figure 14 Changes in tensile yield strength (σ_y), and interfacial shear strength (τ_c) measured with microindentation as a function of rubber content in the interlayer.

dropped up to about 70%, while the yield strength of the interlayer material decreased about 75% (Fig. 14). This confirmed the validity of using the thin interlayer modifications to simulate changes in effective interfacial strength. It also showed that the microindentation test method was quite sensitive to interfacial shear strength, capable of detecting changes in strength reliably.

5. Conclusions

Microindentation has been performed on thin polymer coatings adhering to rigid substrates. The indenter was a cylindrical, flat-ended column. The shear strength between the coating and substrate was studied experimentally and analyzed. As the indenter penetrated into the thin polymer coating, an annular crack could be observed to initiate at the interface at a critical applied stress. For hard coatings, this was directly detectable as a load drop in the load-displacement curve. For soft coatings, the point on the load-displacement curve corresponding to interface failure could be determined by direct observation with an optical microscope during testing.

These observations were analyzed using Agarwal and Raj's shear lag theory to estimate the shear stress at the interface just at the point of failure. This interfacial shear strength has been measured for a variety of polymers and substrates, with repeated tests showing that the results are consistent, with little experimental scatter, and the different systems can be reliably distinguished.

A practical conclusion of the phenomenological observations and mechanical analysis is that the coating thickness which can effectively be tested is approximately equal to the tip diameter, which can be readily changed.

Acknowledgements

The financial support of NSERC, ESTAC and MMO are gratefully acknowledged.

References

1. L. CHENG, X. XIA, W. LU, L. E. SCRIVEN and W. GERBERICH, *J. Poly. Sci B: Physics* **38** (2000) 10.
2. A. G. EVANS and J. W. HUTCHINSON, *Int J. Solids Structures* **20**(5) (1984) 455.
3. D. B. MARSHALL and A. G. EVANS, *J. Appl. Phys.* **56** (1984) 2632.
4. C. ROSSINGTON, A. G. EVANS, D. B. MARSHALL and B. T KHURI-YAKUB, *ibid.* **56** (1984) 2639.
5. M. J. MATTHEWSON, *Appl. Phys. Lett.* **49** (1986) 1426.
6. *Idem.*, in "New Characterization Techniques for Thin Polymer Films," edited by H. Tong and L. T. Nguyen (Wiley, New York, 1990).
7. J. E. RITTER, T. J. LARDNER, L. ROSENFELD and M. R. LIN, *Appl. Phys.* **66** (1989) 3626.
8. M. W. VRATSANOS, E. L. THOMAS and R. J. FARRIS, *J. Mater. Sci.* **22** (1987) 419.
9. S. N. G CHU and J. C. M. LI, *ibid.* **12** (1977) 2200.
10. H. Y. YU and J. C. M. LI, *ibid.* **12** (1977) 2214.
11. F. YANG and J. C. M. LI, *Mech. Mater.* **25** (1997) 163.
12. S. N. G. CHU and J. C. M. LI, *J. Appl. Phys.* **51** (1980) 3338.
13. S. C. WRIGHT, Y. HUANG and N. A. FLECK, *Mech. Mater.* **13** (1992) 277.
14. R. E. BISHOP, R. HILL and N. F. MOTT, *Proc. Phys. Soc.* **57** (1945) 147.
15. Y. LU and D. M. SHINOZAKI, *Mater. Sci. Engin.* A **249** (1998) 134.
16. D. M. SHINOZAKI and Y. LU, *J. Electron. Mater.* **26** (1997) 852.
17. Y. LU and D. M. SHINOZAKI, *Polym. Eng. Sci.* **37** (1997) 1815.
18. R. MOUGINOT and D. MAUGIS, *J. Mater. Sci.* **20** (1985) 4354.
19. I. N. SNEDDON, *Proc. Cambridge Phil. Soc.* **41** (1946) 29.
20. D. TABOR, *Rev. Phys. Technol.* (1970) 145.
21. *Idem.*, in "Microindentation Techniques in Materials Science and Engineering," edited by P. J. Blau and B. R. Lawn (ASTM STP 889, 1986) p. 129.
22. *Idem.*, *Phil. Mag.* A **74** (1996) 1207.
23. P. SARGENT and M. F. ASHBY, *Mater. Sci. Tech.* **8** (1992) 594.
24. Y. LU and D. M. SHINOZAKI, to be published.
25. G. DEHM, M. RUHLE, H. D. CONWAY and R. RAJ, *Acta. Metall.* **45**(2) (1997) 489.
26. D. C. AGARWAL and R. RAJ, *ibid.* **37**(4) (1989) 1265.
27. D. L. ALLARA, F. M. FOWKES, J. NOOLANDI, G. W. RUBLOFF and M. V. TIRRELL, *Mater. Sci. Engin.* **83** (1986) 213.

Received 13 August
and accepted 7 December 2001